Construction and Building Materials 263 (2020) 120218

Contents lists available at ScienceDirect

Construction and Building Materials

journal homepage: www.elsevier.com/locate/conbuildmat

Effects of different silica fume dosages on early-age behavior and cracking resistance of high strength concrete under restrained condition

Dejian Shen [a,b,c,*], Jiacheng Kang [a,b,c], Yang Jiao [a,b,c], Ming Li [a,b,c], Chengcai Li [a,b,c]

[a] College of Civil and Transportation Engineering, Hohai Univ., No. 1, Xikang Rd., Nanjing 210098, China
[b] Jiangsu Engineering Research Center of Crack Control in Concrete, No.1, Xikang Rd., Nanjing 210098, China
[c] Nanjing Engineering Research Center for Prefabricated Construction, No.1, Xikang Rd., Nanjing 210098, China

HIGHLIGHTS

- HSC containing different SF dosages was studied by TSTM.
- Tensile creep and autogenous shrinkage increased as increase of SF dosages.
- Cracking stress or temperature drop decreased as increase of SF dosages.
- Addition of SF decreased the cracking resistance of HSC at early age.

ARTICLE INFO

Article history:
Received 26 February 2020
Received in revised form 23 June 2020
Accepted 8 July 2020
Available online 7 September 2020

Keywords:
High strength concrete
Silica fume
Early age
Temperature Stress Test Machine
Cracking resistance
Tensile creep

ABSTRACT

High strength concrete (HSC) containing silica fume (SF) is widely utilized in construction practices, and its cracking resistance attracts considerable attentions. Previous studies mostly focus on the single parameter of concrete, however, the evaluation of early-age cracking resistance of HSC containing different SF dosages considering different early-age parameters is limited. The present study investigated the effect of different SF dosages on the temperature process, autogenous shrinkage, restrained stress, and creep by utilizing Temperature Stress Test Machine to evaluate the cracking resistance of early-age HSC containing SF. Four concrete mixtures with a 0.33 water/binder ratio were prepared at different replacement levels of SF (0%, 5%, 10%, and 15% of cement by weight). The analysis and experimental results indicated that, when the SF dosage in the HSC increased, (1) the cracking resistance of HSC decreased at early age; (2) the temperature drop, cracking time, cracking stress, and ratio of cracking stress to axial tensile strength decreased; (3) the autogenous shrinkage as well as restrained stress rate increased; (4) the basic tensile creep, specific tensile creep, and creep-shrinkage ratio increased.

1. Introduction

High strength concrete (HSC) with low water/binder (w/b) ratio is widely utilized in construction practices during the past decades due to its high strength and great workability [1–6]. As a kind of industrial by-product composed of much silicon dioxide (SiO_2) [7,8], silica fume (SF) is widely utilized in HSC for many advantages, such as the improvement of compressive strength, elastic modulus, and durability through pozzolanic activity [9,10]. The workability of concrete decreases as increase of SF dosages [11]. HSC containing SF is applied in the designs of high-rise buildings for more usable space, and in the designs of structural bridges for longer spans [10]. However, the low w/b ratio of HSC may cause great self-desiccation and high temperature rise [12,13], which may lead to the development of autogenous shrinkage. The autogenous shrinkage induced by self-desiccation may result in cracking when HSC is under restrained condition [14–16]. Cracking is always a great concern in HSC, and early age is a high occurrence period of cracking [17]. The aggressive substance can penetrate into the concrete through cracks at early age, which may reduce the quality of concrete and damage the security of structures [18–20]. Therefore, the evaluation of early-age cracking resistance of HSC containing SF is important.

Cracking resistance of HSC is influenced by many factors, such as mechanical properties, temperature process, autogenous shrinkage, restrained stress, and creep [9,21]. Restrained stress occurs when shrinkage is under restrained condition and cracks may be observed if restrained stress exceeds the tensile strength of HSC

* Corresponding author at: College of Civil and Transportation Engineering, Hohai Univ., No. 1, Xikang Rd., Nanjing 210098, China.
E-mail address: shendjn@163.com (D. Shen).

https://doi.org/10.1016/j.conbuildmat.2020.120218
0950-0618/

[22]. Restrained stress is not only influenced by shrinkage, but also influenced by creep in concrete [23]. Creep can counteract deformation of concrete and reduce the shrinkage-induced stress, which is able to mitigate the occurrence of cracking [24]. Creep behavior, especially tensile creep, is important for the investigation on the development of deformations and restrained stress in the restrained HSC [25]. The creep occurs when concrete structures are under loading, i.e., the concrete has no immediate elastic response to loads, mainly because the elastic modulus of cement paste is lower than that of coarse aggregate [26]. Creep-related stress relaxation can reduce the self-induced stress caused by shrinkage, which may delay the occurrence of cracking in HSC [27]. In the last few years, several articles have been devoted to the study of early-age behavior and cracking resistance of concrete containing SF. For instance, studies [11,28–30] reveal that the tensile strength and elastic modulus are enhanced by the addition of SF. The influence of the addition of SF on the adiabatic temperature rise and hydration heat is studied in [31,32], which reveals that the addition of SF suppresses adiabatic temperature rise in concrete. Several studies [11,16,33,34] test the autogenous shrinkage of concrete containing SF, and results reveal that the autogenous shrinkage increases as increase of SF dosages. Study [34] reveals that the addition of SF (around 10% cement by weight is replaced by SF) increases the autogenous shrinkage induced restraining stress of HSC with a w/b ratio of 0.33. The early-age tensile creep of concrete under restrained condition is investigated in studies [1,23,35], and results reveal that the tensile creep of HSC containing SF is higher than that of HSC without SF. However, previous studies mostly focus on the single parameter of concrete, such as autogenous shrinkage, creep, and elastic modulus, and the evaluation of early-age cracking resistance of HSC containing different SF dosages considering different early-age parameters is limited. Therefore, investigations on early-age behavior and cracking resistance of HSC containing different dosages of SF are necessary.

Many kinds of cracking tests, such as plate test [14,36], ring test [37–41], and Temperature Stress Test Machine (TSTM) test [42–46], are utilized for the evaluation of shrinkage cracking of concrete [47]. Plate test is mainly based on specimen geometry and fails to calculate the shrinkage-induced stress of concrete [48]. Ring test has been utilized to measure the tensile stress and tensile creep in [49]. However, the determination of tensile stress in ring specimens is difficult because the concrete is inelastic [48]. Besides, ring test cannot provide constant restraint degree, which may affect the creep behavior, stress development, and the cracking resistance of concrete [23]. Ring test is utilized in study [50] for the investigation on restrained shrinkage cracking of concrete with different SF dosages ranging from 0% to 5%, 10%, and 15% by weight of cement, and results reveal that the addition of SF decreases the cracking resistance of concrete. Compared with traditional tests, TSTM can provide various levels of restraint degree and better simulate the working conditions of mass concrete in practice by creating a nearly adiabatic condition [51,52]. Temperature process [53,54], autogenous shrinkage [34,55,56], restrained stress [21], and tensile creep [48,53,57,58] of concrete under uniaxial restrained condition all can be investigated by utilizing TSTM. Studies [1,34] utilize TSTM to investigate the autogenous shrinkage, restrained stress, and tensile creep of HSC containing 0% or 10% SF by weight of cement. However, the investigations utilizing TSTM to evaluate the effect of different SF dosages on the early-age cracking resistance of HSC remain lacking. Therefore, investigations on early-age cracking resistance of HSC containing different dosages of SF by utilizing TSTM are needed to better understand the cracking mechanism of HSC containing different dosages of SF.

The previous investigations on the cracking resistance of HSC at early age can be improved by simultaneously considering temperature process, autogenous shrinkage, restrained stress, and tensile creep under the adiabatic condition [1,12,13,59]. The effect of all relevant factors must be investigated in order to evaluate the cracking resistance of HSC containing different dosages of SF at early age. Therefore, the investigations on temperature process, autogenous shrinkage, restrained stress, and tensile creep of early-age HSC containing different dosages of SF were conducted by utilizing TSTM in the present study.

2. Experimental program

2.1. Materials

P·Ⅱ 52.5R Portland cement with a specific surface area of 375 m^2/kg was utilized conforming to Chinese Standard GB 175 [60] and ASTM C150 [61]. SF utilized in the present study was confirming to ASTM C1240 [62]. The chemical compositions and physical properties of Portland cement and SF are depicted in Table 1. The commercial dry densified SF was utilized in the present study, as reported in [63]. The SF particle is in spherical shape, and the SEM image of the SF is depicted in Fig. 1. The fine aggregate was natural river sand with a fineness modulus of 2.05, as reported in [23,64]. The coarse aggregate was crushed limestone with the maximum aggregate size of 20 mm. A kind of liquid polycarboxylate-based superplasticizer was utilized to improve the rheological properties of concrete, and the results of slump for four mixtures were 130, 128, 127, and 126 mm, respectively.

2.2. Mixture proportions

In the present study, different replacement levels of SF (0%, 5%, 10%, and 15% of cement by weight) were prepared as Mixture SF-00, SF-05, SF-10, and SF-15, as reported in [11,65–67]. Four concrete mixtures were prepared with the same w/b ratio of 0.33, and with the same mixture proportion except the dosage of SF, cement, and superplasticizer, as depicted in Table 2.

2.3. Test details

TSTM system utilized in the present study is a closed-loop test system under uniaxial restrained condition, which is mainly equipped with two molds, controller, linear variable displacement transducer (LVDT), temperature sensor, and load cell [51], as depicted in Fig. 2(a). TSTM was equipped with two same dog-bone shape specimen molds made of aluminum for restrained shrinkage test and free shrinkage test. The center part of the mold was in dimension of 150 mm × 150 mm × 1500 mm, and both ends of specimen mold were in dimension of 150 mm × 280 mm × 160 mm. The ends were utilized for uniform distribution of stress, and the rounded transition areas were set between the center part and two ends of molds, as depicted in Fig. 2(b). The photo of TSTM is depicted in Fig. 2(c).

Table 1
Chemical compositions and physical properties of Portland cement and silica fume.

Item	Portland cement	Silica fume
SiO_2 (%)	19.90	92.60
Al_2O_3 (%)	4.60	0.82
Fe_2O_3 (%)	3.00	0.48
CaO (%)	64.60	0.34
MgO (%)	0.78	1.44
SO_3 (%)	2.37	0.47
Na_2O (%)	0.06	0.40
K_2O (%)	0.65	1.22
Specific surface area (m^2/kg)	375	18700

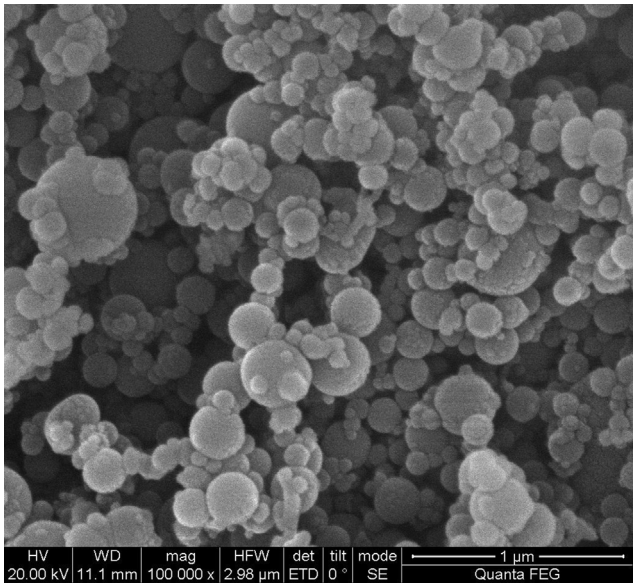

Fig. 1. The SEM image of commercial dry densified silica fume.

In the restrained specimen, the gripped end was connected to an LVDT, which was utilized to record the displacement of restrained specimen, and the other end was fixed to the steel frame. TSTM can provide different degrees of restraint by pulling or pushing the gripped end of restrained specimen through a stepper motor [23,68]. A load cell was utilized to record the stress process of concrete. The temperature process of both restrained shrinkage specimen and free shrinkage specimen was recorded by the temperature sensors, and the temperature was controlled by the liquid circulating in the molds, as reported in [1,26,48,69]. The deformation of free shrinkage specimen was recorded by the LVDT connected to the free end.

2.4. Testing procedure

Fresh concrete was poured into two specimen molds immediately after mixing. Plastic film sheets were placed in molds before pouring to diminish the friction between concrete and molds, as reported in [21,53]. The surfaces of HSC specimens were sealed immediately after pouring in order to reduce the moisture evaporation. Temperature sensors were inserted into free and restrained specimens directly after pouring, respectively. The temperature process of mass concrete can be considered to be the adiabatic condition in practice because the heat of core concrete cannot escape into surroundings easily [70,71]. Therefore, HSC specimens were cured and tested under the adiabatic condition in the present study to better simulate the temperature process of mass concrete, as reported in [52,59,67,72]. Temperature of HSC increased to peak temperature, and then maintained for 36 h by heating circulating liquids in the molds. Finally, the temperature cooled at a rate of 1°C/h until specimens cracked. The cooling rate was not too fast nor too slow in order to minimize the visco-elastic influence and prevent the thermal gradients, as reported in [73].

2.5. Strength and modulus

HSC specimens were cured and tested conforming to Chinese Standard GB/T 50081 [74] in order to determine the mechanical properties of that. The average value of the results tested by three 150 mm cubic HSC specimens was utilized to determine the compressive strength and splitting tensile strength, and elastic modulus was obtained based on the average value of three HSC prisms in dimension of 150 mm × 150 mm × 300 mm. Electro-hydraulic Servo Universal Testing Machine was utilized to test the mechanical properties of HSC specimens.

The elastic modulus in tension of concrete is considered to be equal to that in compression at early age [75–77]. Tensile elastic modulus of HSC is determined by Eq. (1) [78].

$$E_t(t) = E_{t,28}\exp\left\{-\lambda_1[\ln(1+(t-t_0))]^{-k_1}\right\} \quad (1)$$

in which $E_t(t)$ = time-dependent tensile elastic modulus, in GPa; $E_{t,28}$ = 28-d tensile elastic modulus, in GPa; t = age of concrete after pouring, in day; t_0 = initial setting time of concrete, in day; and λ_1, k_1 = fitting parameters.

Based on the results of splitting tensile strength, axial tensile strength is approximately determined by Eqs. (2) and (3) [78,79].

$$f_t = 0.77 \times f_{spl} + 0.21 \quad (2)$$

$$f_t(t) = f_{t,28}\exp\left\{-\lambda_2[\ln(1+(t-t_0))]^{-k_2}\right\} \quad (3)$$

in which f_t = axial tensile strength, in MPa; f_{spl} = splitting tensile strength, in MPa; $f_t(t)$ = time-dependent axial tensile strength, in MPa; $f_{t,28}$ = 28-d axial tensile strength, in MPa; and λ_2, k_2 = fitting parameters.

2.6. Autogenous shrinkage measurement

Autogenous shrinkage of HSC is defined by the self-desiccation volume change when the temperature of concrete maintains unchanged [80]. Value of autogenous shrinkage is determined by subtracting the thermal deformation from the total deformation of HSC specimens by Eqs. (4) and (5) [81].

$$\varepsilon_{as} = \varepsilon_{total} - \varepsilon_T \quad (4)$$

$$\varepsilon_T = \alpha \times \Delta T \quad (5)$$

in which ε_{total} = total deformation, in με; ε_{as} = autogenous shrinkage deformation, in με; ε_T = thermal deformation, in με; α = coefficient of thermal expansion (CTE), in με/°C; and ΔT = temperature change, in °C.

CTE is determined by Eq. (6) considering that it changes drastically along with time [23].

Table 2
Mixture proportions of high strength concrete.

Mixture composition (kg/m^3)	SF-00	SF-05	SF-10	SF-15
Water	158.4	158.4	158.4	158.4
Cement	480	456	432	408
Silica fume	0	24	48	72
Fine aggregate	620	620	620	620
Coarse aggregate	1160	1160	1160	1160
Superplasticizer	2.40	2.88	3.84	4.80

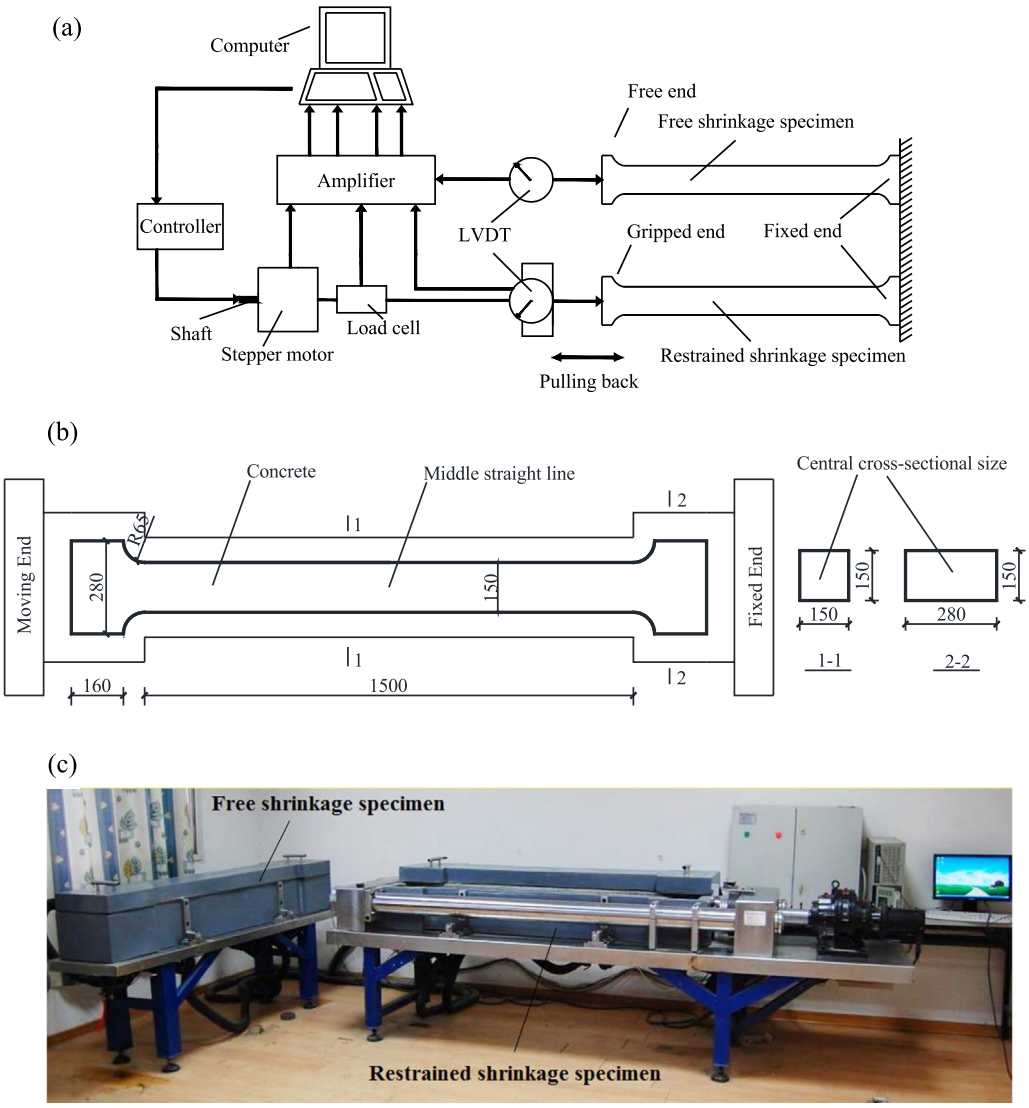

Fig. 2. The schematic diagrams of TSTM: (a) the schematic diagram of TSTM [1]; (b) the schematic diagram of restrained shrinkage specimens (mm); (c) the photo of TSTM.

$$\alpha_T(t) = \alpha_k \times (1 + 41 \times t^{-m}) \quad (6)$$

+in which $\alpha_T(t)$ = time-dependent CTE, in με/°C; α_k = 28-d CTE, in με/°C; and $m = 2.0$.

The value of CTE was basically stable within 1 d, as reported in [23,82]. The value of α_k was nearly determined by the linear regression analysis result of the deformation-temperature curve during cooling phase, which was 6.44, 6.30, 6.13, and 7.10 °C for Mixture SF-00, SF-05, SF-10, and SF-15, respectively. The autogenous shrinkage is determined by Eq. (7) [81].

$$\varepsilon_{as}(t) = \varepsilon_{total} - \alpha_T(t) \times [T(t) - T_{time-zero}] \quad (7)$$

in which $\varepsilon_{as}(t)$ = time-dependent autogenous shrinkage deformation, in με; $T(t)$ = time-dependent temperature, in °C; and $T_{time-zero}$ = time-zero temperature, in °C.

3. Test results and discussion

3.1. Effect of SF on strength and modulus of HSC

The 28-d cubic compressive strength of four HSC mixtures was 60.9, 66.5, 71.9, and 73.9 MPa, which increased by 9.20%, 18.06%, and 21.35% as increase of SF dosages ranging from 0% to 5%, 10%, and 15%, respectively. The results were compatible with previous findings [11,29,83] regarding cubic compressive strength. The main reason was that the addition of SF improved the bond strength between aggregates and paste, and enhanced the microstructure of concrete.

The results and predicting models of elastic modulus and axial tensile strength at 3, 7, and 28 d after pouring for four HSC mixtures are depicted in Table 3 and Fig. 3, respectively, and the coefficients of determination (R^2) were all greater than 0.990. The 28-d axial tensile strength or 28-d elastic modulus of four HSC mixtures was 3.84, 4.09, 4.31, and 4.38 MPa or 50.4, 52.9, 55.7, and 56.4 GPa, which increased by 6.51%, 12.24%, and 14.06% or 4.96%, 10.52%, and 11.90% as increase of SF dosages ranging from 0% to 5%, 10%, and 15%, respectively. The results were compatible with previous findings [11,28] regarding tensile strength, and the results were compatible with previous findings [29,30] regarding elastic modulus.

The enhancement of tensile strength and elastic modulus was able to be explained in three aspects. For one thing, the SF particles are extremely small, and the SF particles fit into the spaces between cement grains in the concrete, which is of great significance in pore-size refinement and matrix densification in the concrete [84]. What is more, SF reacts with calcium hydroxide formed

Table 3
Elastic modulus and axial tensile strength for four mixtures.

Concrete mixtures	Elastic modulus (GPa)			λ_1	k_1	Axial tensile strength (MPa)			λ_2	k_2
	3 d	7 d	28 d			3 d	7 d	28 d		
SF-00	46.5	48.9	50.4	0.169	2.617	3.28	3.55	3.84	0.298	2.194
SF-05	48.3	52.0	52.9	0.271	3.915	3.49	3.75	4.09	0.292	2.065
SF-10	51.6	53.8	55.7	0.148	2.311	3.78	4.05	4.31	0.252	2.259
SF-15	51.8	54.4	56.4	0.169	2.418	3.85	4.13	4.38	0.251	2.318

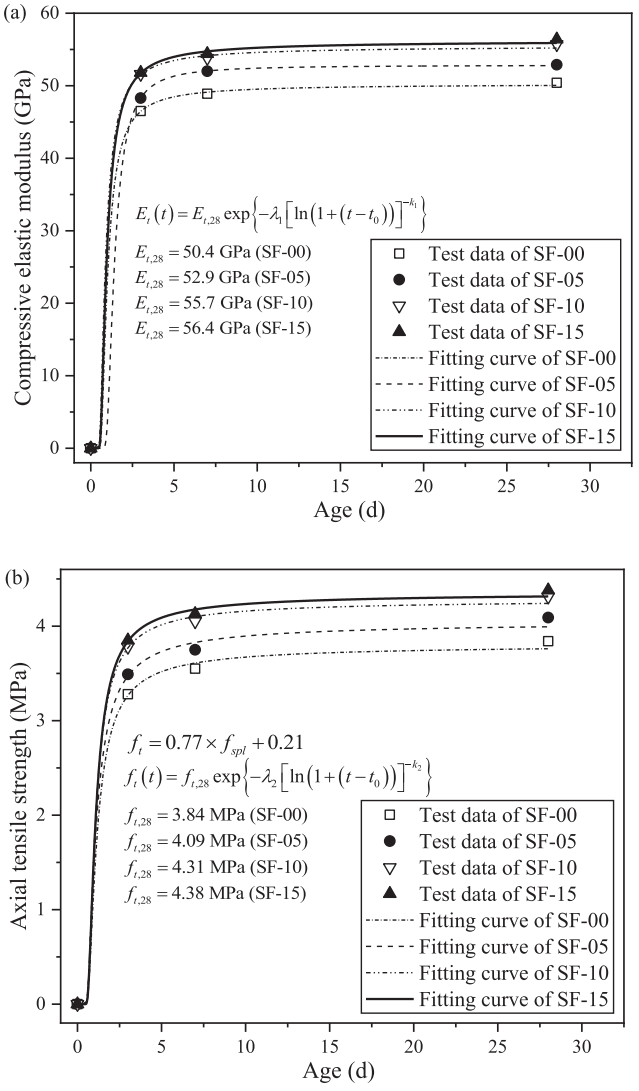

Fig. 3. Experimental results and predicting models of elastic modulus and axial tensile strength of four mixtures.

during hydration and provides additional calcium silicate hydrates (C-S-H) [10,85], which may improve the strength of early-age concrete [2]. One final point is, the addition of SF increases the bond strength between the aggregates and paste in concrete effectively [86], makes the microstructure of concrete dense, and decreases the total porosity, which is of great significance in increasing strength and elastic modulus [87,88].

3.2. Effect of SF on temperature process of HSC

The cracking resistance is directly affected by the temperature process of concrete [27]. The hydration reactions of cement inside concrete lead to the liberation of heat at early age, which will cause temperature rise of HSC specimens [89,90]. The temperature of concrete rises quickly at the early stage after pouring due to great cement hydration [91]. The pouring temperature or peak temperature was 14.2, 13.9, 14.6, and 14.5 °C or 55.3, 52.4, 52.5, and 51.8 °C for Mixture SF-00, SF-05, SF-10, and SF-15, respectively, as depicted in Fig. 4(a). Adiabatic temperature rise is determined by Eq. (8) [21].

$$T_{tr} = T_{ht} - T_{ct} \tag{8}$$

in which T_{tr} = adiabatic temperature rise, in °C; T_{ht} = peak temperature, in °C; and T_{ct} = pouring temperature, in °C. The adiabatic temperature rise was 41.1, 38.5, 37.9, and 37.3 °C for

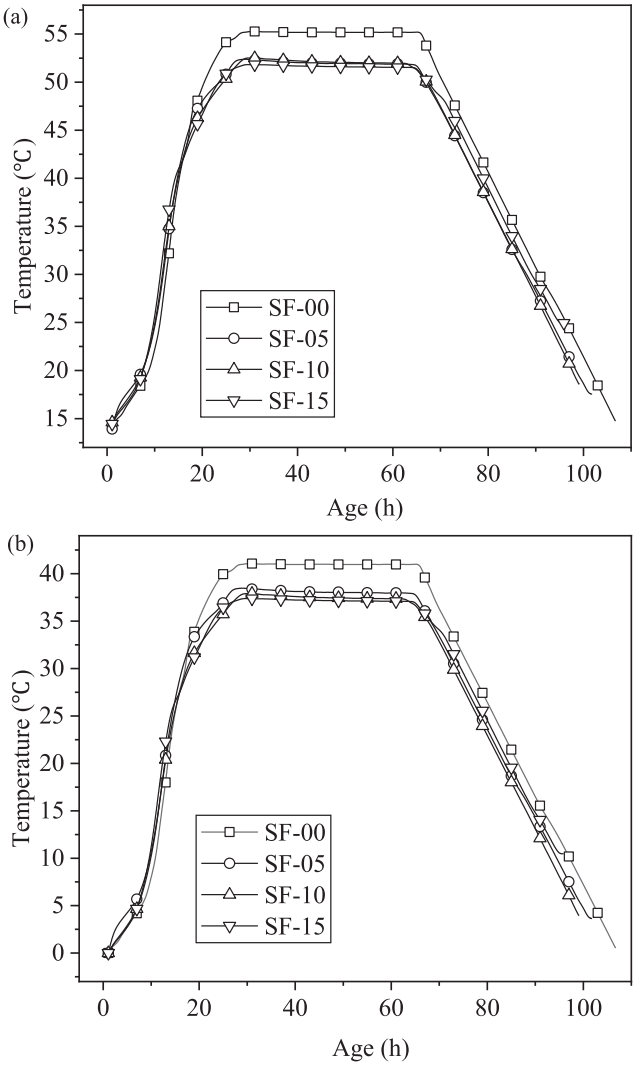

Fig. 4. Temperature process of free shrinkage concrete specimens: (a) actual temperature process; (b) absolute temperature rise and drop.

Mixture SF-00, SF-05, SF-10, and SF-15, which decreased by 6.33%, 7.79%, and 9.25% as increase of SF dosages ranging from 0% to 5%, 10%, and 15%, respectively, as depicted in Fig. 4(b). The results were compatible with previous findings [31,32] regarding adiabatic temperature rise. One possible reason is that the heat liberated by SF is less than Portland cement per gram [32]. The dosage of cement decreased as increase of SF dosages, and the decrease of cement reduced the total heat in HSC. Therefore, the adiabatic temperature rise of HSC decreased as increase of SF dosages.

The tensile stress occurs when the concrete is under restrained condition during cooling phase, which may lead to concrete cracking and reduce the structural durability [80]. Therefore, the cracking temperature and temperature drop are important elements for the investigation on the cracking resistance of HSC [20,90]. Results of temperature drop are determined by Eq.(9) [49].

$$T_{td} = T_{ht} - T_{ck} \tag{9}$$

in which T_{td} = temperature drop of HSC, in °C; T_{ht} = peak temperature, in °C; and T_{ck} = cracking temperature of HSC, in °C.

The cracking temperature or the temperature drop was 14.7, 17.5, 18.6, and 24.9 °C or 40.6, 34.9, 33.9, and 26.9 °C for Mixture SF-00, SF-05, SF-10, and SF-15, which increased by 19.05%, 26.53%, and 69.39% or decreased by 14.04%, 16.50%, and 33.74% as increase of SF dosages ranging from 0% to 5%, 10%, and 15%, respectively, as depicted in Fig. 5. Results of temperature drop indicated that the thermal cracking resistance of HSC decreased as increase of SF dosages, as reported in [49].

3.3. Effect of SF on autogenous shrinkage of HSC

Free deformation of HSC includes autogenous deformation and thermal deformation [92], which cannot be measured immediately after pouring [16,93–100]. The autogenous deformation is measured from time-zero, and there is no general consensus in the literature on the definition of time-zero, which is determined in several ways based on the setting time [93], onset of internal RH drop [94], onset of capillary pressure [95], transition point from the autogenous strain curve [96], rate of deformation [100] and so on [55,97–99,101]. Time-zero was normally several hours after the beginning of the test and the elastic modulus at that time was large enough so that restrained stress could be induced by autogenous shrinkage. Considering that only stress-induced deformation was analysed in the present study, the value of autogenous shrinkage was set to be zero at the moment when stress occurred in the TSTM test, as reported in [55]. Measurements were started after pouring and stress development could be recorded by the load cell. The addition of SF decreased the expansion of concrete, as depicted in Fig. 6. The maximum free deformation of HSC specimens was 189, 143, 115, and 73 με, which decreased by 24.34%, 39.15%, and 61.38% as increase of SF dosages ranging from 0% to 5%, 10%, and 15%, respectively. The main reason is that the pozzolanic reaction between portlandite and SF reduces the alkali ions and then decreases the pH in the pore solution, which suppresses the expansion caused by alkali-aggregate reactivity [102]. The autogenous shrinkage of HSC increased slightly and the thermal deformation of that nearly unchanged during the phase when the temperature of concrete maintained constant, which caused a slight decrease of total deformation in HSC specimens. In addition, the absolute value of free shrinkage increased as increase of SF dosages, as depicted in Fig. 6.

The addition of SF increased autogenous shrinkage of HSC, as depicted in Fig. 7. The mixture SF-15 cracked first at 96 h after pouring, the autogenous shrinkage of Mixture SF-00, SF-05, SF-10, and SF-15 at 96 h was −121, −161, −201, and −286 με, the absolute value of which increased by 33.06%, 66.12%, and 136.36% as increase of SF dosages ranging from 0% to 5%, 10%, and 15%, respectively. The absolute value of autogenous shrinkage increased nonlinearly as increase of SF dosages. The results were compatible with previous findings [11,33] regarding autogenous shrinkage. The main reason is that the average pore diameter as well as porosity is reduced by the addition of SF [103], which increases the capillary tension and hence causes more shrinkage in the concrete due to the refinement of micro-pore structure [10,104,105]. In addition, the SF reacts with the $Ca(OH)_2$ formed by hydration, accelerates the hydration rate of cementitious materials, and accelerates the consumption of free water in the pores of concrete, which may cause self-desiccation and lead to the increase of autogenous shrinkage [106].

In the present study, the curing conditions and temperature processes of TSTM tests and mechanical properties tests were different. Therefore, the actual age of restrained specimens are converted to the equivalent time of 20 °C by Eq. (10) [107].

$$t_e = \int_0^t \exp\left[\frac{E_a(T)}{R}\left(\frac{1}{T_{ref}+273} - \frac{1}{T(t)+273}\right)\right] dt \tag{10}$$

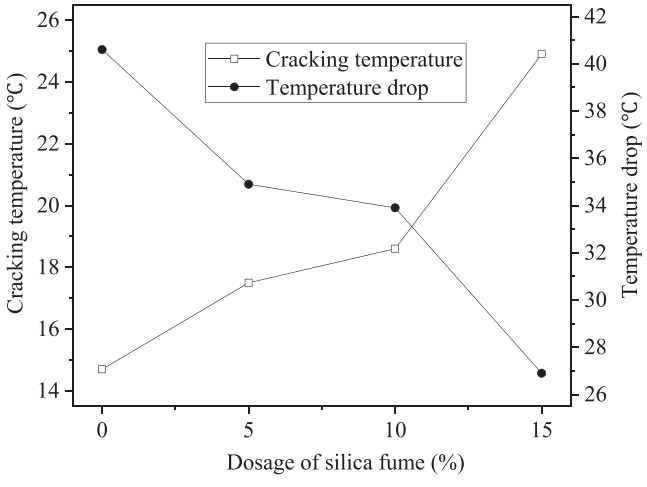

Fig. 5. Relationship between cracking temperature or temperature drop and dosage of silica fume.

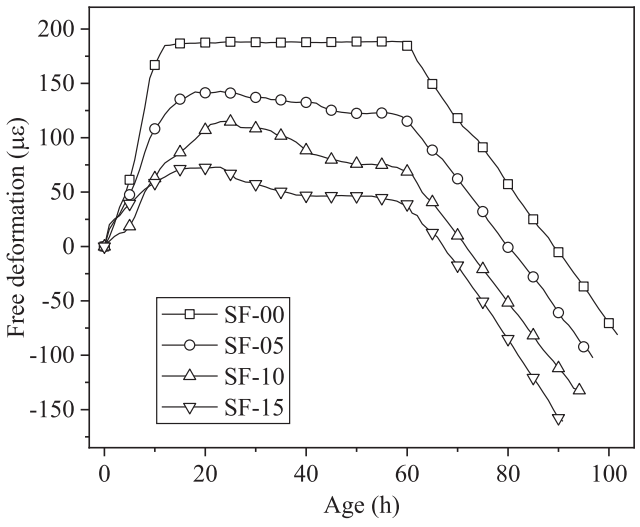

Fig. 6. The free deformation of concrete specimens.

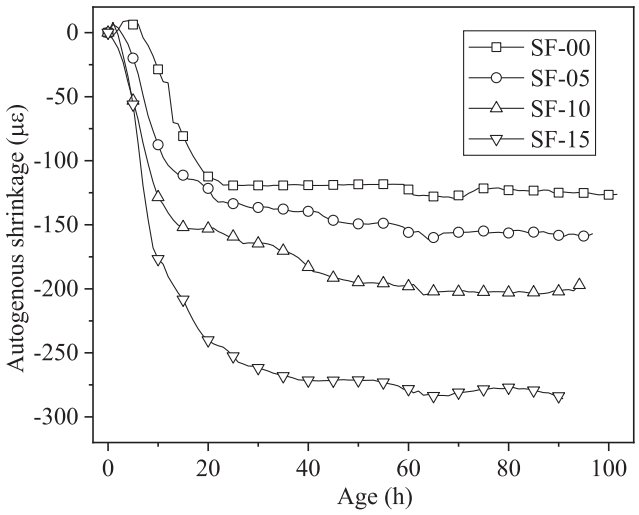

Fig. 7. Autogenous shrinkage of concrete specimens.

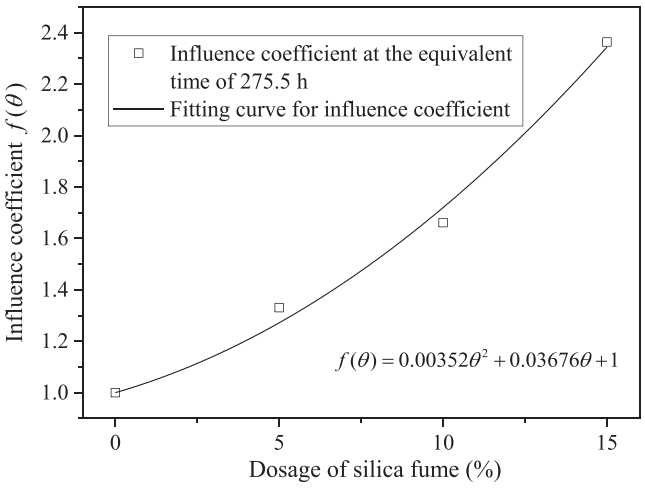

Fig. 8. The influence coefficient at the equivalent time of 275.5 h of four mixtures.

in which t_e = equivalent time of 20 °C; $T(t)$ = actual temperature, in °C; $E_a(T)$ = activation energy, in kJ/mol ($T(t) \geqslant 20$°C, $E_a(T) = 33.5$ kJ/mol; $T(t) < 20$°C, $E_a(T) = 33.5 + 1.47(20 - T(t))$ kJ/mol); R = an ideal gas constant (8.315 J · mol^{-1} · K^{-1}); and T_{ref} = a reference temperature (20 °C).

The equivalent time of concrete is determined in the discrete form by Eq. (11) [107].

$$t_e = \sum \exp\left[\frac{E_a(T)}{R}\left(\frac{1}{T_{ref}+273} - \frac{1}{T(t)+273}\right)\right]\Delta t \tag{11}$$

The cracking time or the equivalent cracking time was 107, 102, 99, and 96 h or 315.3, 280.5, 277.2, and 275.5 h for Mixture SF-00, SF-05, SF-10, and SF-15, respectively.

In the present study, a modified model on the basis of Tazawa-Miyazawa model was proposed to predict the effect of SF dosages on autogenous shrinkage of HSC, as given in Eqs. (12) [108].

$$\begin{cases} \varepsilon_{cas}(t_e) = \varepsilon_{cas0}(\theta)\beta_a(t_e) \\ \beta_a(t_e) = 1 - \exp(-a \cdot {t_e}^b) \\ \varepsilon_{cas0}(\theta) = \varepsilon_{cas0}(0) \cdot f(\theta) \\ f(\theta) = \lambda_3\theta^2 + k_3\theta + 1 \end{cases} \tag{12}$$

in which $\varepsilon_{cas}(t_e)$ = equivalent time-dependent autogenous shrinkage, in με; $\varepsilon_{cas0}(\theta)$ = autogenous shrinkage at the equivalent time of 275.5 h for four mixtures, in με; $\beta_a(t_e)$ = development coefficient of autogenous shrinkage; θ = SF replacement level of cement by weight, in %; a, b = fitting parameters; $\varepsilon_{cas0}(0)$ = autogenous shrinkage of mixture SF-00 at the equivalent time of 275.5 h (-121 με); $f(\theta)$ = influence coefficient of autogenous shrinkage; and λ_3, k_3 = fitting parameters.

The results of λ_3, k_3 are depicted in Fig. 8, and the coefficient of determination (R^2) was 0.989. The average values of fitting parameters were a = 0.854 and b = 1.231, respectively. The model to predict the effect of SF dosages on autogenous shrinkage of HSC was determined by Eq. (13).

$$\varepsilon_{cas}(t_e) = \varepsilon_{cas0}(0) \cdot \left(0.00352\theta^2 + 0.03676\theta + 1\right) \cdot \left[1 - \exp\left(-0.854 \times {t_e}^{1.231}\right)\right] \tag{13}$$

The results of experiments and the predicting model are depicted in Fig. 9. The proposed model could be utilized to predict the effect of SF dosages on autogenous shrinkage of HSC. The proposed model could predict the autogenous shrinkage of HSC with a w/b ratio of 0.33 containing different SF dosages ranging from 0% to 15% by weight of cement.

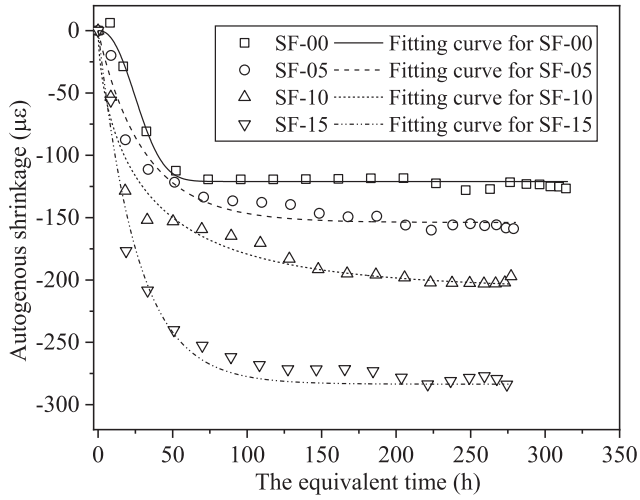

Fig. 9. Predicting model on autogenous shrinkage over the equivalent time of four mixtures.

3.4. Effect of SF on restrained stress of HSC

The value of maximum restrained compressive stress was 1.92, 0.93, 0.76, and 0.68 MPa, which decreased by 51.56%, 60.42%, and 64.58% as increase of SF dosages ranging from 0% to 5%, 10%, and 15%, respectively, as depicted in Fig. 10. At the time when temperature of HSC reached a maximum value, the strength and elastic modulus of HSC were still at a low level, which would cause stress relaxation if HSC specimens suffered high compressive stress simultaneously, as reported in [109]. The temperature of concrete maintained for 36 h and the decreasing speed of the compressive stress turned slower when the strength of concrete developed during this period, as depicted in Fig. 11.

During cooling phase, zero-stress occurred when restrained compressive stress changed to tensile one, and temperature of that time was defined as zero-stress temperature ($T_{zero-stress}$), as reported in [53], and then, restrained tensile stress of HSC developed due to temperature drop and high rate of shrinkage. When values of restrained stress reach tensile strength of HSC specimens,

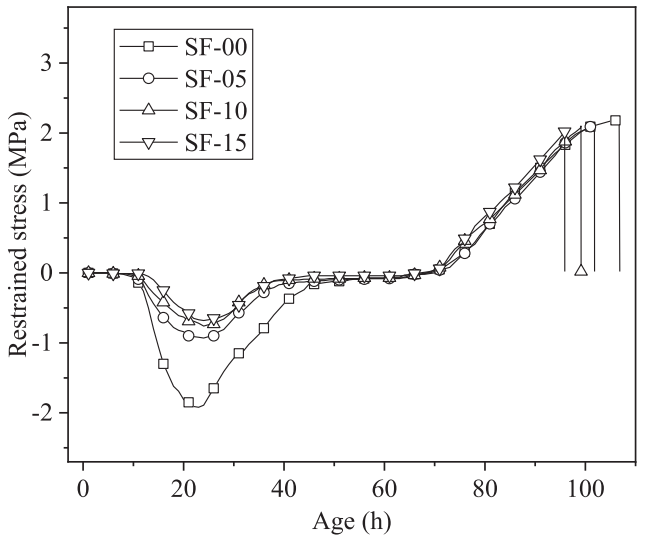

Fig. 10. The development process of restrained stress in restrained concrete specimens.

cracking may occur [68], which is indicated by a sharp drop in stress curves depicted in Fig. 11 [27]. Cracking stress of Mixture SF-00, SF-05, SF-10, and SF-15 was 2.20, 2.12, 2.10, and 2.02 MPa at the cracking time, and the cracking stress decreased by 3.64%, 4.55%, and 8.18% as increase of SF dosages ranging from 0% to 5%, 10%, and 15%, respectively, which indicated that the addition of SF decreased the cracking resistance of HSC. The results were compatible with previous findings [50] regarding cracking time. Meanwhile, the results of restrained tensile stress rate were 0.055, 0.059, 0.063, and 0.066 MPa/h, which increased by 7.27%, 14.55%, and 20.00% as increase of SF dosages ranging from 0% to 5%, 10%, and 15%, respectively, as depicted in Fig. 12. The results revealed that the restrained tensile stress in specimens developed as increase of SF dosages.

Considering that the cracking stress of four mixtures was unable to evaluate the cracking resistance adequately because the values of tensile strength at cracking time of four mixtures were different, the investigation on ratio of restrained stress to axial tensile strength at the equivalent cracking time was conducted in the present study, as reported in [27]. The axial tensile strength at the equivalent cracking time of Mixture SF-00, SF-05, SF-10, and SF-15 was 3.71, 3.92, 4.18, and 4.25 MPa, respectively. Therefore, ratio of cracking stress to axial tensile strength was 0.59, 0.54, 0.50, and 0.48, which decreased by 8.47%, 15.25%, and 18.64% as increase of SF dosages ranging from 0% to 5%, 10%, and 15%, respectively, which indicated that the cracking occurred when the restrained stress was lower than the axial tensile strength of HSC. The main reason is that HSC specimens are exposed to sustained loading, which causes static fatigue and damage accumulation [110]. The results revealed that the addition of SF decreased the cracking resistance of HSC. A partial explanation for this may lie in the fact that, when the autogenous shrinkage of HSC is under restrained condition at early age, the generation of internal stress occurs and may cause a premature tensile failure in HSC [34].

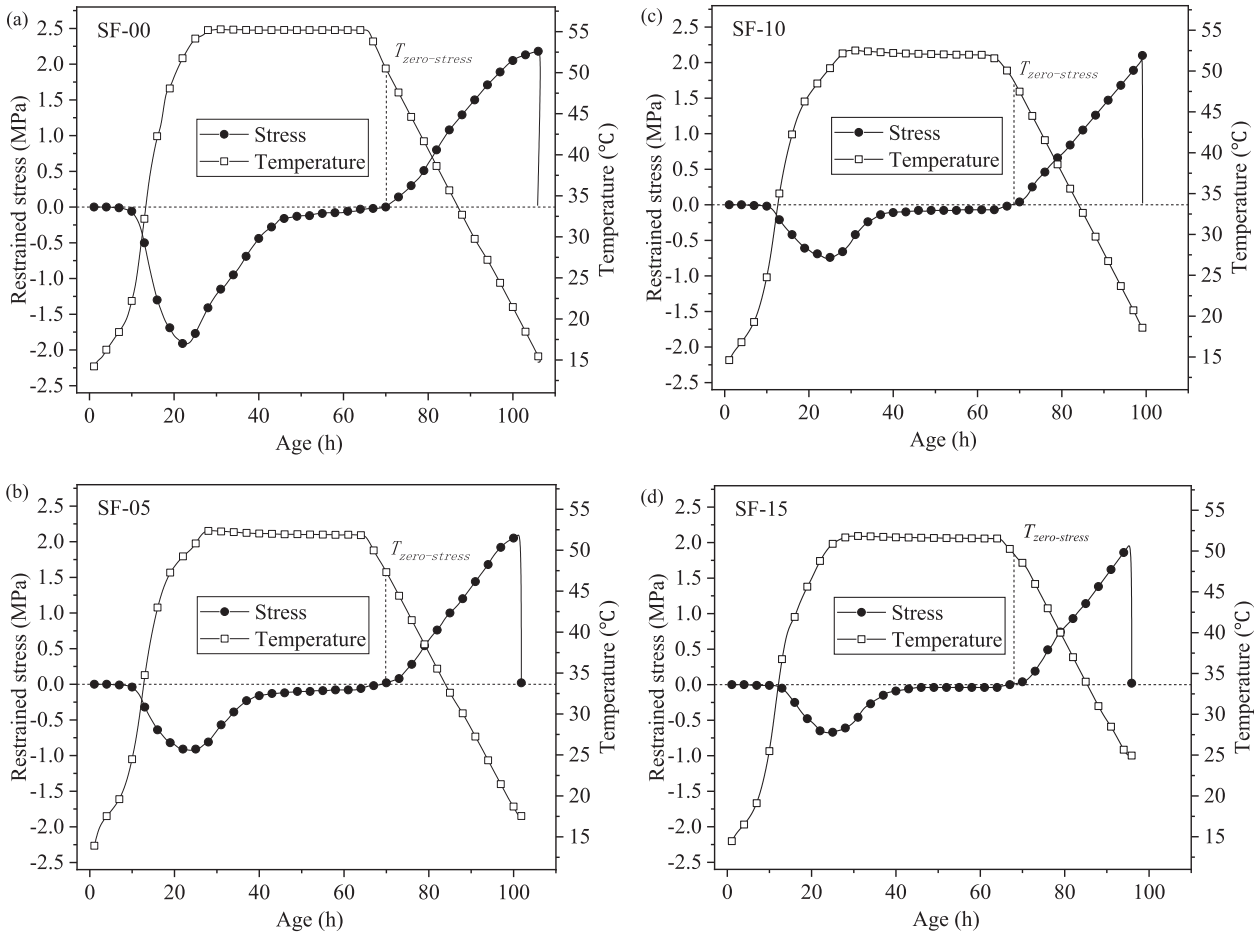

Fig. 11. Temperature process and restrained stress of four mixtures.

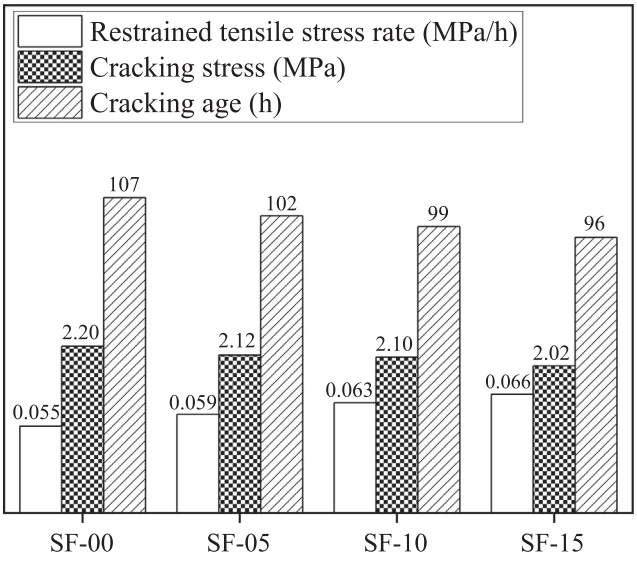

Fig. 12. Cracking time, cracking stress, and restrained tensile stress rate of four mixtures.

The addition of SF caused more autogenous shrinkage in HSC, which induced more internal stress when the HSC specimens were under restrained condition, and resulted in lower cracking resistance.

3.5. Effect of SF on tensile creep of HSC

Considering that the HSC specimens were nearly under a complete sealing condition, the present study utilized the basic tensile creep, specific tensile creep, and the creep-shrinkage ratio to evaluate the visco-elastic properties of HSC, as reported in [23]. Total strain of restrained specimens is the sum of free strain, creep strain, and elastic strain [1]. The total strain was zero considering that the specimen was under full restrained condition, as given in Eq. (14).

$$\varepsilon_{total} = \varepsilon_e + \varepsilon_{sh} + \varepsilon_{cr} = 0 \quad (14)$$

in which ε_{total} = total strain of restrained specimen, in με; ε_{sh} = free strain of free shrinkage specimen, in με; ε_e = accumulation of incremental elastic strain, in με; and ε_{cr} = creep strain, in με.

The restrained tensile stress developed during cooling phase because the shrinkage of specimen was under restrained condition, which increased the basic tensile creep of the specimen. The basic tensile creep was defined to be zero at the time when the restrained tensile stress first occurred during cooling phase in the present study, as reported in [68]. The basic tensile creep at 96 h was 123, 124, 132, and 153 με, which increased by 0.81%, 7.32%, and 24.39% as increase of SF dosages ranging from 0% to 5%, 10%, and 15%, respectively, as depicted in Fig. 13. The results revealed that development of basic tensile creep with time was rapid and almost linear, and basic tensile creep increased as increase of SF dosages, which were compatible with previous findings [1,23,35] regarding tensile creep.

Specific tensile creep, i.e., ratio of basic tensile creep strain to restrained stress, in με/MPa, is utilized to normalize various stresses of four mixtures [1]. The specific basic tensile creep was defined as the ratio of cumulative basic tensile creep to restrained stress considering that restrained stress was not constant in the present study, as reported in [21,23]. Restrained stress at 96 h was 1.85, 1.86, 1.88, and 2.02 MPa, and the specific tensile creep for Mixture SF-00, SF-05, SF-10, and SF-15 at 96 h was 66.49, 66.67, 70.21, and 75.74 με/MPa, which increased by 0.27%, 5.59%, and 13.91% as increase of SF dosages ranging from 0% to 5%, 10%, and 15%, respectively. The specific tensile creep increased nonlinearly as increase of SF dosages. The results revealed that the addition of SF increased the visco-elastic properties of HSC with same w/b ratio under restrained condition, and the basic tensile creep increased nonlinearly as SF dosages increased.

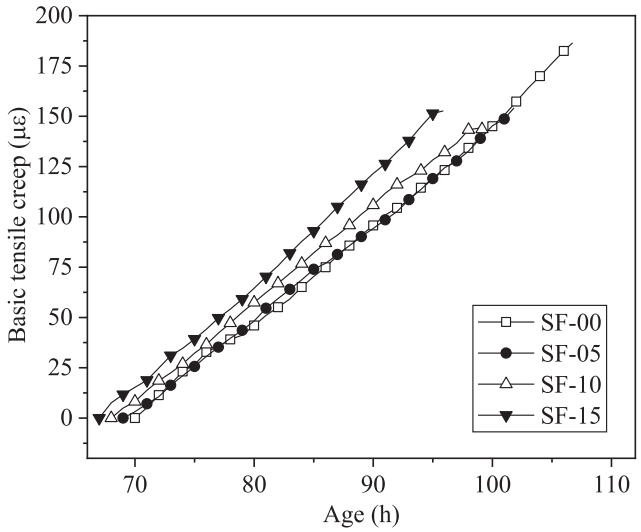

Fig. 13. Basic tensile creep of four mixtures.

Creep-shrinkage ratio was the ratio of the basic tensile creep strain to total free shrinkage strain, which was utilized to reflect the tensile strain reduction in concrete, as reported in [23,27]. The total free shrinkage strain at 96 h was 160, 160, 166, and 189 με, and the creep-shrinkage ratio at 96 h was 0.77, 0.78, 0.80, and 0.81 for Mixture SF-00, SF-05, SF-10, and SF-15, respectively. The creep-shrinkage ratio of specimen increased when the SF dosages increased, as depicted in Fig. 14. The creep-shrinkage ratio represents the degree of stress relaxation in specimens, and results reveal that the addition of SF increases the creep, as well as degree of stress relaxation in specimens [23].

In the present study, the development of tensile creep in HSC containing SF under restrained condition was different from traditional understanding that the addition of SF would decrease the

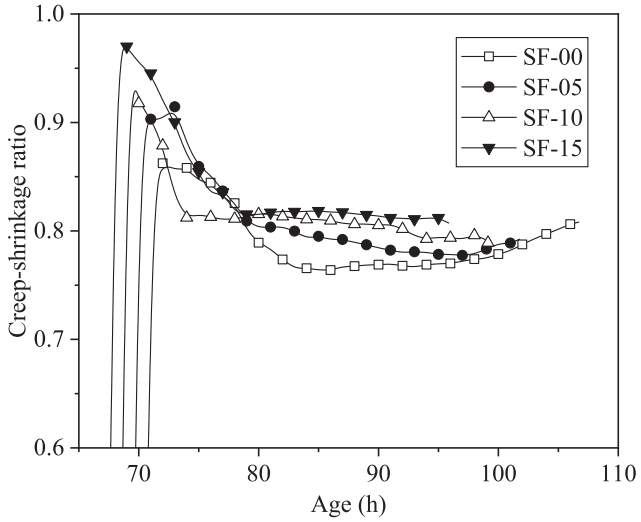

Fig. 14. Creep-shrinkage ratio of four mixtures.

creep of concrete due to its low porosity and high stiffness. The results were compatible with previous findings [1,23] regarding tensile creep. A possible explanation for this might be that the addition of SF increased the autogenous shrinkage of concrete, and the times that the restrained specimen was pulled back to original length increased in TSTM test, which may induce the increase of the number of microcracks in concrete [21]. The tensile creep of concrete will increase when the number of microcracks increases under tensile condition [110]. Thus, the addition of SF increased the tensile creep of concrete under restrained condition.

3.6. Effect of SF on cracking resistance of HSC

Many single criterions or integrated criterions, such as temperature drop, cracking stress, cracking time, ratio of cracking stress to axial tensile strength, and integrated criterion of cracking potential, are adopted to evaluate cracking behavior of concrete [20,27,80,90]. Therefore, in order to better evaluate early-age cracking resistance of HSC containing different dosages of SF, single criterions and integrated criterions were both adopted in the present study.

The net time of cracking and tensile stress rate at cracking time were proposed by ASTM C1581 [111] to investigate cracking resistance. The results of net time of cracking were 1.70, 1.54, 1.42, and 1.29 d for Mixture SF-00, SF-05, SF-10, and SF-15, respectively. An integrated criterion of cracking potential modified in [14,21,54] on the basis of [111,112] was adopted to evaluate the early-age cracking resistance of HSC containing different dosages of SF, as given in Eq. (15).

$$\varphi_N = \frac{S}{t_{tcr}} \tag{15}$$

in which $\varphi_N =$ integrated criterion of cracking potential, in MPa/(h·day); $S =$ tensile stress rate, in MPa/h; and $t_{tcr} =$ net time of cracking from the starting point of tensile stage to the cracking time, in day.

The results of integrated criterion of cracking potential was 0.032, 0.038, 0.044, and 0.051 MPa/(h·day) for Mixture SF-00, SF-05, SF-10, and SF-15, which increased by 18.75%, 37.50%, and 59.38% as increase of SF dosages ranging from 0% to 5%, 10%, and 15%, respectively, as depicted in Fig. 15. The results on integrated criterion of cracking potential revealed that the addition of SF decreased the cracking resistance of HSC, which was compatible with previous findings [50].

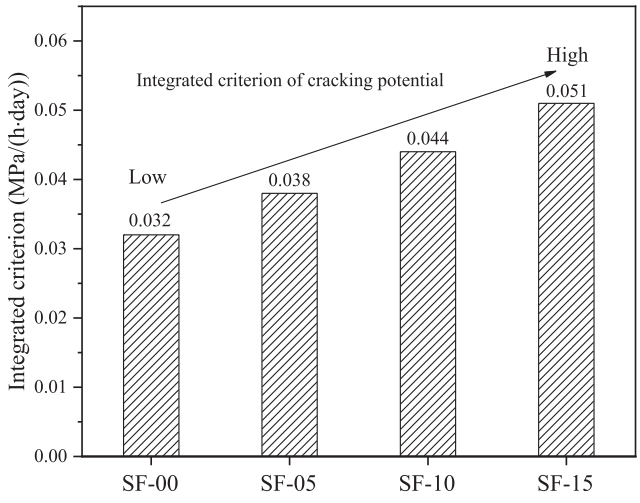

Fig. 15. Integrated criterion of cracking potential of four mixtures.

4. Conclusions

The present study revealed the effect of SF on early-age behavior and cracking resistance of HSC under restrained condition. Tests and analysis on temperature process, autogenous shrinkage, restrained stress, and tensile creep of HSC for Mixture SF-00, SF-05, SF-10, and SF-15 were conducted, respectively. Based on the experiment findings, following conclusions were obtained:

(1) The addition of SF increased the compressive strength, splitting tensile strength, and elastic modulus of HSC at early age.

(2) The addition of SF considerably affected the early-age behavior of HSC. Generally, the cracking temperature, autogenous shrinkage, and the restrained stress rate increased, while the temperature drop, cracking time, cracking stress, and ratio of cracking stress to axial tensile strength of HSC decreased as increase of SF dosages ranging from 0% to 5%, 10%, and 15%, respectively.

(3) The basic tensile creep, specific tensile creep, and creep-shrinkage ratio of HSC increased as increase of SF dosages ranging from 0% to 5%, 10%, and 15%, respectively.

(4) The early-age cracking resistance of HSC decreased as increase of SF dosages. The integrated criterion of cracking potential was 0.032, 0.038, 0.044, and 0.051MPa/(h · day), which revealed that the cracking resistance of HSC under restrained condition decreased as increase of SF dosages ranging from 0% to 5%, 10%, and 15%, respectively.

CRediT authorship contribution statement

Dejian Shen: Conceptualization, Methodology, Project administration. **Jiacheng Kang:** Investigation, Writing - original draft, Writing - review & editing, Formal analysis. **Yang Jiao:** Investigation, Validation. **Ming Li:** Writing - original draft, Validation, Formal analysis. **Chengcai Li:** Formal analysis.

Declaration of Competing Interest

The authors declare that they have no known competing financial interests or personal relationships that could have appeared to influence the work reported in this paper.

Acknowledgements

The financial support of the National Natural Science Foundation of China (Grant No. 51879092) is gratefully acknowledged. The support of the Fundamental Research Funds for the Central Universities (Grant No. 2019B52814) is also gratefully acknowledged. The Postgraduate Research & Practice Innovation Program of Jiangsu Province (Grant Nos. KYCX20_0454 and SJCX20_0166) is gratefully acknowledged. This work is also sponsored by Qing Lan Project of Jiangsu Province of China.

References

[1] K. Kolver, S. Igarashi, A. Bentur, Tensile creep behavior of high strength concretes at early ages, Mater. Struct. 32 (5) (1999) 383–387.
[2] B. Langan, K. Weng, M. Ward, Effect of silica fume and fly ash on heat of hydration of Portland cement, Cem. Concr. Res. 32 (7) (2002) 1045–1051.
[3] D.J. Shen, X.Z. Liu, B.Z. Zhou, X. Zeng, J. Du, Influence of initial cracks on the frequency of a 60-year-old reinforced concrete box beam, Mag. Concr. Res. (2019), https://doi.org/10.1680/jmacr.18.00276.
[4] D.J. Shen, C.Y. Wen, P.F. Zhu, Y.H. Wu, J.J. Yuan, Influence of Barchip fiber on early-age autogenous shrinkage of high strength concrete, Constr. Build. Mater. 256 (2020) 119223.
[5] D.J. Shen, C.C. Li, Z.Z. Feng, C.Y. Wen, B. Ojha, Influence of strain rate on bond behavior of concrete members reinforced with basalt fiber-reinforced polymer rebars, Constr. Build. Mater. 228 (2019) 116755.
[6] D.J. Shen, C.Y. Wen, P.F. Zhu, M. Li, B. Ojha, C.C. Li, Bond behavior between basalt fiber-reinforced polymer bars and concrete under cyclic loading, Constr. Build. Mater. 258 (2020) 119518.

[7] E. Villar-Cociña, L. Rodier, H. Savastano, M. Lefrán, M.F. Rojas, A comparative study on the pozzolanic activity between bamboo leaves ash and silica fume: kinetic parameters, Waste Biomass Valorization (2019) 1–8.
[8] I. Sharaky, F. Megahed, M. Seleem, A. Badawy, The influence of silica fume, nano silica and mixing method on the strength and durability of concrete, SN Applied Sciences 1 (6) (2019) 575–584.
[9] E. Güneyisi, M. Gesoğlu, S. Karaoğlu, K. Mermerdaş, Strength, permeability and shrinkage cracking of silica fume and metakaolin concretes, Constr. Build. Mater. 34 (2012) 120–130.
[10] R. Siddique, M.I. Khan, Supplementary cementing materials, Springer Science & Business, Media (2011) 67–120.
[11] M. Mazloom, A.A. Ramezanianpour, J.J. Brooks, Effect of silica fume on mechanical properties of high-strength concrete, Cem. Concr. Compos. 26 (4) (2004) 347–357.
[12] D.P. Bentz, K.A. Snyder, Protected paste volume in concrete: Extension to internal curing using saturated lightweight fine aggregate, Cem. Concr. Res. 29 (11) (1999) 1863–1867.
[13] D. Cusson, T. Hoogeveen, An experimental approach for the analysis of early-age behaviour of high-performance concrete structures under restrained shrinkage, Cem. Concr. Res. 37 (2) (2007) 200–209.
[14] D.J. Shen, C. Liu, J.L. Jiang, J.C. Kang, M. Li, Influence of super absorbent polymers on early-age behavior and tensile creep of internal curing high strength concrete, Constr. Build. Mater. (2020) 120068, https://doi.org/10.1016/j.conbuildmat.2020.120068.
[15] D.J. Shen, J.C. Kang, X.J. Yi, L.K. Zhou, X. Shi, Effect of double hooked-end steel fiber on early-age cracking potential of high strength concrete in restrained ring specimens, Constr. Build. Mater. 223 (2019) 1095–1105.
[16] M.S. Meddah, M. Suzuki, R. Sato, Influence of a combination of expansive and shrinkage-reducing admixture on autogenous deformation and self-stress of silica fume high-performance concrete, Constr. Build. Mater. 25 (1) (2011) 239–250.
[17] T. Voigt, G. Ye, Z. Sun, S.P. Shah, K. Van Breugel, Early age microstructure of Portland cement mortar investigated by ultrasonic shear waves and numerical simulation, Cem. Concr. Res. 35 (5) (2005) 858–866.
[18] D.P. Bentz, M.A. Peltz, J. Winpigler, Early-age properties of cement-based materials. ii: influence of water-to-cement ratio, J. Mater. Civ. Eng. 21 (9) (2009) 512–517.
[19] D.J. Shen, C. Liu, M.L. Wang, X.C. Jin, H. Tang, Prediction model for internal relative humidity in early-age concrete under different curing humidity conditions, Constr. Build. Mater (2020) 119987, https://doi.org/10.1016/j.conbuildmat.2020.119987.
[20] D.J. Shen, W.T. Wang, J.W. Liu, X.G. Zhao, G.Q. Jiang, Influence of Barchip fiber on early-age cracking potential of high performance concrete under restrained condition, Constr. Build. Mater. 187 (2018) 118–130.
[21] D.J. Shen, J.L. Jiang, M.Y. Zhang, P.P. Yao, G.Q. Jiang, Tensile creep and cracking potential of high performance concrete internally cured with super absorbent polymers at early age, Constr. Build. Mater. 165 (2018) 451–461.
[22] E.I. Yang, S. Morita, S.T. Yi, Effect of axial restraint on mechanical behavior of high-strength concrete beams, Struct J 97 (5) (2000) 751–756.
[23] T. Zhang, W.Z. Qin, Tensile creep due to restraining stresses in high-strength concrete at early ages, Cem. Concr. Res. 36 (3) (2006) 584–591.
[24] L. Østergaard, D.A. Lange, S.A. Altoubat, H. Stang, Tensile basic creep of early-age concrete under constant load, Cem. Concr. Res. 31 (12) (2001) 1895–1899.
[25] I. Khan, A. Castel, R.I. Gilbert, Tensile creep and early-age concrete cracking due to restrained shrinkage, Constr. Build. Mater. 149 (2017) 705–715.
[26] Z.F. Zhao, K.J. Wang, D.A. Lange, H.G. Zhou, W.L. Wang, D.M. Zhu, Creep and thermal cracking of ultra-high volume fly ash mass concrete at early age, Cem. Concr. Compos. 99 (2019) 191–202.
[27] D.J. Shen, C. Liu, C.C. Li, X.G. Zhao, G.Q. Jiang, Influence of Barchip fiber length on early-age behavior and cracking resistance of concrete internally cured with super absorbent polymers, Constr. Build. Mater. 214 (2019) 219–231.
[28] B. Sabir, High-strength condensed silica fume concrete, Mag. Concr. Res. 47 (172) (1995) 219–226.
[29] Q.L. Wang, J.C. Bao, Effect of silica fume on mechanical properties and carbonation resistance of concrete, Appl Mech Mater 238 (3) (2012) 161–164.
[30] A.A. Almusallam, H. Beshr, M. Maslehuddin, O.S. Al-Amoudi, Effect of silica fume on the mechanical properties of low quality coarse aggregate concrete, Cem. Concr. Compos. 26 (7) (2004) 891–900.
[31] P.L. Ng, W.W.S. Fung, J.J. Chen, A.K.H. Kwan, Adiabatic temperature rise of condensed silica fume (CSF) concrete, Adv. Mater. Res. 261–263 (2011) 788–795.
[32] R.P. Lohtia, R.C. Joshi, Mineral admixtures, Concrete admixtures handbook, William Andrew Publishing, 1996, pp. 657–739.
[33] M.H. Zhang, C.T. Tam, M.P. Leow, Effect of water-to-cementitious materials ratio and silica fume on the autogenous shrinkage of concrete, Cem. Concr. Res. 33 (10) (2003) 1687–1694.
[34] S. Igarashi, A. Bentur, K. Kovler, Autogenous shrinkage and induced restraining stresses in high-strength concretes, Cem. Concr. Res. 30 (11) (2000) 1701–1707.
[35] B. Bissonnette, M. Pigeon, Tensile creep at early ages of ordinary, silica fume and fiber reinforced concretes, Cem. Concr. Res. 25 (5) (1995) 1075–1085.
[36] P. Soroushian, F. Mirza, A. Alhozajiny, Plastic shrinkage cracking of polypropylene fiber reinforced concrete, Mater J 92 (5) (1993) 553–560.
[37] D.J. Shen, K.Q. Liu, C.Y. Wen, Y.Q. Shen, G.Q. Jiang, Early-age cracking resistance of ground granulated blast furnace slag concrete, Constr. Build. Mater. 222 (2019) 278–287.
[38] W.J. Weiss, W. Yang, S.P. Shah, Shrinkage cracking of restrained concrete slabs, J. Eng. Mech. 124 (7) (1998) 765–774.
[39] D.J. Shen, Y. Jiao, J.C. Kang, Z.Z. Feng, Y.Q. Shen, Influence of ground granulated blast furnace slag on early-age cracking potential of internally cured high performance concrete, Constr. Build. Mater. 233 (2020) 117083.
[40] D.J. Shen, Z.Z. Feng, J.C. Kang, C.Y. Wen, H.F. Shi, Effect of Barchip fiber on stress relaxation and cracking potential of concrete internally cured with super absorbent polymers, Constr. Build. Mater. 249 (2020) 118392.
[41] D.J. Shen, C.Y. Wen, J.C. Kang, H.F. Shi, Z.L. Xu, Early-age stress relaxation and cracking potential of high-strength concrete reinforced with Barchip fiber, Constr. Build. Mater. 258 (2020) 119538.
[42] C.H. Jiang, Y. Yang, M.A. Chengchang, N.I. Tongyuan, Evaluation of anti-cracking performance for concrete based on temperature-stress test and analytic hierarchy process, J Chin Ceram Soc 43 (8) (2015) 1017–1023 (in Chinese).
[43] A.E. Klausen, T. Kanstad, Ø. Bjøntegaard, E. Sellevold, Comparison of tensile and compressive creep of fly ash concretes in the hardening phase, Cem. Concr. Res. 95 (2017) 188–194.
[44] J.D. Xin, G.X. Zhang, Y. Liu, Z.H. Wang, Z. Wu, Effect of temperature history and restraint degree on cracking behavior of early-age concrete, Constr. Build. Mater. 192 (2018) 381–390.
[45] H. Zhu, Y. Hu, Q.B. Li, R. Ma, Restrained cracking failure behavior of concrete due to temperature and shrinkage, Constr. Build. Mater. 244 (2020) 118318.
[46] D.J. Shen, X.Z. Liu, X. Zeng, X.G. Zhao, G.Q. Jiang, Effect of polypropylene plastic fibers length on cracking resistance of high performance concrete at early age, Constr. Build. Mater. 244 (2020) 117874.
[47] A. Bentur, K. Kovler, Evaluation of early age cracking characteristics in cementitious systems, Mater. Struct. 36 (3) (2003) 183–190.
[48] K. Kovler, Testing system for determining the mechanical behaviour of early age concrete under restrained and free uniaxial shrinkage, Mater. Struct. 27 (6) (1994) 324–330.
[49] K. Raoufi, J. Schlitter, D.P. Bentz, W.J. Weiss, Parametric assessment of stress development and cracking in internally cured restrained mortars experiencing autogenous deformations and thermal loading, Adv Civ Eng (2011) 1–16.
[50] J.T. Ding, Z.J. Li, Effects of metakaolin and silica fume on properties of concrete, Mater J 99 (4) (2002) 393–398.
[51] D.H. Nguyen, V.T. Nguyen, P. Lura, V.T. Dao, Temperature-stress testing machine-A state-of-the-art design and its unique applications in concrete research, Cem. Concr. Compos. 102 (2019) 28–38.
[52] T.J. Barrett, I. De la Varga, W.J. Weiss, Reducing cracking in concrete structures by using internal curing with high volumes of fly ash, Structures Congress (2012) 699–707.
[53] Y. Wei, W. Hansen, Tensile creep behavior of concrete subject to constant restraint at very early ages, J. Mater. Civ. Eng. 25 (9) (2012) 1277–1284.
[54] D.J. Shen, J.L. Jiang, J.X. Shen, P.P. Yao, G.Q. Jiang, Influence of prewetted lightweight aggregates on the behavior and cracking potential of internally cured concrete at an early age, Constr. Build. Mater. 99 (2015) 260–271.
[55] P. Lura, K. Van Breugel, I. Maruyama, Effect of curing temperature and type of cement on early-age shrinkage of high-performance concrete, Cem. Concr. Res. 31 (12) (2001) 1867–1872.
[56] Bjøntegaard Ø. Basis for and practical approaches to stress calculations and crack risk estimation in hardening concrete structures–State of the art. Norwegian Public Roads Administration 2011.
[57] T. Aly, J.G. Sanjayan, Shrinkage-cracking behavior of OPC-fiber concrete at early-age, Mater. Struct. 43 (6) (2010) 755–764.
[58] T. Aly, J.G. Sanjayan, Shrinkage cracking properties of slag concretes with one-day curing, Mag. Concr. Res. 60 (1) (2008) 41–48.
[59] D. Cusson, W.L. Repette, Early-age cracking in reconstructed concrete bridge barrier walls, ACI Mater. J. 97 (4) (2000) 438–446.
[60] GB 175-2007, Common portlad cement. National cement Standardization Technical Committee, 2007 (in Chinese).
[61] ASTM C150 / C150M-20, Standard Specification for Portland Cement, ASTM International, West Conshohocken, PA, 2020.
[62] ASTM C1240-20, Standard Specification for Silica Fume Used in Cementitious Mixtures, ASTM International, West Conshohocken, PA, 2020.
[63] S. Diamond, S. Sahu, N. Thaulow, Reaction products of densified silica fume agglomerates in concrete, Cem. Concr. Res. 34 (9) (2004) 1625–1632.
[64] M. Ekenel, J.J. Myers, Durability performance of bridge concretes, Part II: high-strength concrete (HSC), J. ASTM Int. 2 (7) (2005) 1–12.
[65] M. Khan, A. Rehman, M. Ali, Efficiency of silica-fume content in plain and natural fiber reinforced concrete for concrete road, Constr. Build. Mater. 244 (2020) 118382.
[66] M. Mazloom, Estimating long-term creep and shrinkage of high-strength concrete, Cem. Concr. Compos. 30 (4) (2008) 316–326.
[67] V. Giner, S. Ivorra, F. Baeza, E. Zornoza, B. Ferrer, Silica fume admixture effect on the dynamic properties of concrete, Constr. Build. Mater. 25 (8) (2011) 3272–3277.
[68] D.J. Shen, W.T. Wang, Q.Y. Li, P.P. Yao, G.Q. Jiang, Early-age behaviour and cracking potential of fly ash concrete under restrained condition, Mag. Concr. Res. 72 (5) (2020) 246–261.

[69] D.J. Shen, Y. Jiao, Y. Gao, S.S. Zhu, G.Q. Jiang, Influence of ground granulated blast furnace slag on cracking potential of high performance concrete at early age, Constr. Build. Mater. 241 (2020) 117839.
[70] B.H. Oh, S.C. Choi, S.W. Cha, Temperature and relative humidity analysis in early-age concrete decks of composite bridges, Monitoring and Modeling Concrete Properties, Springer, Measuring, 2006, pp. 305–316.
[71] K. Tang, S. Millard, G. Beattie, Technical and economic aspects of using GGBFS for crack control mitigation in long span reinforced concrete structures, Constr. Build. Mater. 39 (2013) 65–70.
[72] ACI Committee 207, Effect of restraint, volume change and reinforcement on cracking of mass concrete, 1995.
[73] J. Schlitter, D.P. Bentz, W.J. Weiss, Quantifying stress development and remaining stress capacity in restrained, internally cured mortars, ACI Mater. J. 110 (1) (2013) 3–11.
[74] GB/T 50081-2019, Standard for test methods of concrete physical and mechanical properties. Ministry of Housing and Urban-Rural Development of the People Republic of China, 2019 (in Chinese).
[75] P. Lura, Autogenous deformation and internal curing of concrete, Dup Sci (2003).
[76] H.T. See, E.K. Attiogbe, M.A. Miltenberger, Shrinkage cracking characteristics of concrete using ring specimens, Mater J 100 (3) (2003) 239–245.
[77] T. Wee, H. Lu, S. Swaddiwudhipong, Tensile strain capacity of concrete under various states of stress, Mag. Concr. Res. 52 (3) (2000) 185–193.
[78] T. Kanstad, T.A. Hammer, Ø. Bjøntegaard, E.J. Sellevold, Mechanical properties of young concrete: Part II: Determination of model parameters and test program proposals, Mater. Struct. 36 (4) (2003) 226–230.
[79] T. Kanstad, T.A. Hammer, Ø. Bjøntegaard, E.J. Sellevold, Mechanical properties of young concrete: Part I: Experimental results related to test methods and temperature effects, Materials Structures 36 (4) (2003) 218–225.
[80] D.J. Shen, C. Liu, Z.Z. Feng, S.S. Zhu, C. Liang, Influence of ground granulated blast furnace slag on the early-age anti-cracking property of internally cured concrete, Constr. Build. Mater. 223 (2019) 233–243.
[81] I. Chu, S.H. Kwon, M.N. Amin, J.K. Kim, Estimation of temperature effects on autogenous shrinkage of concrete by a new prediction model, Constr. Build. Mater. 35 (2012) 171–182.
[82] M. Viviani, B. Glisic, I. Smith, Separation of thermal and autogenous deformation at varying temperatures using optical fiber sensors, Cem. Concr. Compos. 29 (6) (2007) 435–447.
[83] E. Güneyisi, M. Gesoğlu, T. Özturan, Properties of rubberized concretes containing silica fume, Cem. Concr. Res. 34 (12) (2004) 2309–2317.
[84] ACI Committee 234, Guide for the use of silica fume in concrete, 2006.
[85] A. Mardani-Aghabaglou, G.İ. Sezer, K. Ramyar, Comparison of fly ash, silica fume and metakaolin from mechanical properties and durability performance of mortar mixtures view point, Constr. Build. Mater. 70 (2014) 17–25.
[86] R. Siddique, Utilization of silica fume in concrete: Review of hardened properties, Resour. Conserv. Recycl. 55 (11) (2011) 923–932.
[87] Z.Q. Zhang, B. Zhang, P.Y. Yan, Comparative study of effect of raw and densified silica fume in the paste, mortar and concrete, Constr. Build. Mater. 105 (2016) 82–93.
[88] H. Du, K.H. Tan, Properties of high volume glass powder concrete, Cem. Concr. Compos. 75 (2016) 22–29.
[89] P. Lura, J. Bisschop, On the origin of eigenstresses in lightweight aggregate concrete, Cem. Concr. Compos. 26 (5) (2004) 445–452.
[90] D.J. Shen, X.Z. Liu, Q.Y. Li, L. Sun, W.T. Wang, Early-age behavior and cracking resistance of high-strength concrete reinforced with Dramix 3D steel fiber, Constr. Build. Mater. 196 (2019) 307–316.
[91] A. Schackow, C. Effting, I.R. Gomes, I.Z. Patruni, F. Vicenzi, C. Kramel, Temperature variation in concrete samples due to cement hydration, Appl. Therm. Eng. 103 (2016) 1362–1369.
[92] D. Cusson, T. Hoogeveen, Internal curing of high-performance concrete with pre-soaked fine lightweight aggregate for prevention of autogenous shrinkage cracking, Cem. Concr. Res. 38 (6) (2008) 757–765.
[93] A. Darquennes, S. Staquet, B. Espion, Determination of time-zero and its effect on autogenous deformation evolution, Eur J Environ Civ En 15 (7) (2011) 1017–1029.
[94] H. Huang, G. Ye, Examining the "time-zero" of autogenous shrinkage in high/ultra-high performance cement pastes, Cem. Concr. Res. 97 (2017) 107–114.
[95] Y. Ma, X. Yang, J. Hu, Z. Zhang, H. Wang, Accurate determination of the "time-zero" of autogenous shrinkage in alkali-activated fly ash/slag system, Compos. B Eng. 177 (2019) 107367.
[96] J.R. Tenório Filho, P. Gomes, M.A. de Araújo, D. Snoeck, N. De Belie, Discussing different approaches for the time-zero as start for autogenous shrinkage in cement pastes containing superabsorbent polymers, Mater 12 (18) (2019) 2962–2977.
[97] M. Meddah, P.-C. Aïtcin, N. Petrov, A new approach for the determination of the starting point of autogenous shrinkage strains (ASS), Spec. Publ. 234 (2006) 473–484.
[98] S. Eppers, C. Mueller, Autogenous shrinkage and time-zero of UHPC determined with the shrinkage cone, Proceed. Concr. 8 (2008) 709–714.
[99] C.W. Miao, Q. Tian, J.P. Liu, W. Sun, Very early age self-desiccation effect measurement based on meniscus depression technology for concrete, J Chin Ceram Soc 35 (4) (2007) 509.
[100] M.S. Meddah, A. Tagnit-Hamou, Evaluation of rate of deformation for early-age concrete shrinkage analysis and time zero determination, J. Mater. Civ. Eng. 23 (7) (2011) 1076–1086.
[101] A. Bentur, Early-age shrinkage and cracking in cementitious systems, Concr. Sci. Eng. 3 (2001) 3–12.
[102] M.A. Bérubé, J. Duchesne, Does silica fume merely postpone expansion due to alkali-aggregate reactivity?, Constr Build. Mater. 7 (3) (1993) 137–143.
[103] S.I. Igarashi, A. Watanabe, M. Kawamura, Evaluation of capillary pore size characteristics in high-strength concrete at early ages, Cem. Concr. Res. 35 (3) (2005) 513–519.
[104] Brooks JJ, Cabrera JG, Johari MM, Factors affecting the autogenous shrinkage of silica fume high-strength concrete. Proceedings, International workshop on Autogenous Shrinkage of Concrete. Hiroshima: Japan Concrete Institute; June 1998, pp. 185-192.
[105] Y. Li, J. Bao, Y. Guo, The relationship between autogenous shrinkage and pore structure of cement paste with mineral admixtures, Constr. Build. Mater. 24 (10) (2010) 1855–1860.
[106] M. Jensen, P.F. Hansen, Autogenous deformation and change of the relative humidity in silica fume-modified cement paste, ACI Mater. J. 93 (6) (1996) 539–543.
[107] Krauß M, Rostásy FS, Gutsch AW, Modelling of degree of hydration on basis of adiabatic heat release, IPACS REPORT BE96-3843, 2001:13.
[108] E. Tazawa, S. Miyazawa, Influence of cement and admixture on autogenous shrinkage of cement paste, Cem. Concr. Res. 25 (2) (1995) 281–287.
[109] P.K. Mehta, P.J.M. Monteiro, Concrete: Microstructure, Properties, and Materials, thired ed., Mcgraw-Hill, New York, 2006.
[110] S.A. Altoubat, D.A. Lange, Creep, shrinkage, and cracking of restrained concrete at early age, ACI Mater. J. 98 (4) (2001) 323–331.
[111] ASTM C1581 / C1581M-18a, Standard Test Method for Determining Age at Cracking and Induced Tensile Stress Characteristics of Mortar and Concrete under Restrained Shrinkage, ASTM International, West Conshohocken, PA, 2018.
[112] K. Kovler, A. Bentur, Cracking sensitivity of normal- and high-strength concretes, ACI Mater. J. 106 (6) (2009) 537–542.